Finite element simulations for natural convective flow of nanofluid in a rectangular cavity having corrugated heated rods

Naeem Ullah[1] · Sohail Nadeem[2,3] · Arif Ullah Khan[4]

Abstract

In this study, numerical simulations of natural convection in a partially heated rectangular cavity containing water-based copper oxide nanofluid (CuO–water) have been carried out. The flow field and heat transfer inside the cavity are influenced by two corrugated heated rods. The governing partial differential equations are transformed to dimensionless coupled nonlinear partial differential equations using some suitable variables. For the thermophysical properties of nanofluid, Koo and Kleinstreuer–Li model is implemented in the governing equation. Numerical solutions of the resulting system of equations are obtained utilizing finite element method. The simulations for flow field and thermal distribution are portrayed in terms of line graphs, streamlines and isotherms. The results are executed for various Rayleigh numbers ($10^4 \leq \mathrm{Ra} \leq 10^6$), nanoparticle volume fractions ($0.0 \leq \phi \leq 0.2$), amplitudes of the corrugated heated rods ($0.05 \leq A_\mathrm{m} \leq 0.2$) and wavelength numbers ($0 \leq n \leq 20$). Results depict that the thermal distribution and flow field are getting stronger because of increasing Ra and n. The impact of nanoparticle volume fraction is found to be useful in intensifying the heat transfer rate because of dominant convection. It is worth mentioning that with an increase in A_m the thermal distribution in the entire cavity is control by convection.

Keywords Rectangular cavity · Natural convection · Nanofluid · Corrugated heated rods · Finite element method

List of symbols

$\bar{x}, \bar{y}$	Dimensional Cartesian coordinates [L]
$\bar{u}, \bar{v}$	Velocity components $\left[\mathrm{L\,T^{-1}}\right]$
g	Gravitational acceleration $\left[\mathrm{L\,T^{-2}}\right]$
U, V	Dimensionless velocity components
k	Thermal conductivity $\left[\mathrm{ML\,K^{-1}T^{-3}}\right]$
C_p	Specific heat capacity $\left[\mathrm{ML^2\,K^{-1}T^{-2}}\right]$
Ra	Rayleigh number
Nu	Dimensionless number
ω	Frequency of the wavy rods $\left[\mathrm{T^{-1}}\right]$
n_1	Dimensionless wavelength number
X, Y	Dimensionless variable
$\bar{P}$	Pressure $\left[\mathrm{M\,L^{-1}\,T^{-2}}\right]$
$\bar{T}$	Temperature [K]
T	Dimensionless temperature
l	Length of cavity [L]
Pr	Prandtl number
P	Dimensionless pressure
$\mathrm{Nu_m}$	Mean Nusselt number
λ	Amplitude of inner rods [L]
A_m	Amplitude ratio

Greek symbols

μ	Dynamic viscosity $\left[\mathrm{M\,L^{-1}T^{-1}}\right]$
β	Thermal expansion coefficient $\left[\mathrm{K^{-1}}\right]$
ϕ	Nanoparticle volume fraction
ν	Kinematic viscosity $\left[\mathrm{L^{-2}\,T^{-1}}\right]$
ρ	Density $\left[\mathrm{M\,L^{-3}}\right]$
γ	Penalty parameter

Subscripts

f	Fluid
C	Cold
nf	Nanofluid
h	Hot

✉ Sohail Nadeem
sohail.nadeem@tdtu.edu.vn

1 Department of Mathematics, Quaid i Azam University, Islamabad, Pakistan

2 Faculty of Mathematics and Statistics, Ton Duc Thang University, Ho Chi Minh City, Vietnam

3 Mathematics and its Applications in Life Sciences Research Group, Ton Duc Thang University, Ho Chi Minh City, Vietnam

4 Department of Mathematics, Gomal University, D.I. Khan 29050, Khyber Pakhtunkhwa, Pakistan

Introduction

Heat transfer through natural convection finds its applications in many industrial and engineering process. Particularly, in chemical and nuclear reactors, energy conversion, metallurgical process, cooling of electronic devices, solar energy collector, lakes and reservoir, building insulation materials, food processing, etc. In various geometrical shapes, investigations of natural convection have significant importance to technological and industrial development. Researchers have performed and presented theoretical, experimental and numerical methodologies to explore the flow field and thermal properties considering natural convection in different cavities and enclosures. Plenty of research has been done by many researchers in this field. Sheikholeslami et al. [1] discussed the natural convection in circular cavity which contains a sinusoidal heated obstacle; the simulations show that the amplitude of the inner heated object and Rayleigh number strongly influenced the thermal and flow characteristics. The impact of natural convection on flow distribution in an inclined cavity having porous medium is investigated by Wu and Wang [2]. They incorporated the results for thermal and time periodic boundary conditions. Aparna and Seetharamu [3] analyzed the natural convective flow in a trapezoidal cavity under the effect of thermally variable boundary. They reported that under the impact of constant temperature the heat transfer rate rises as compared to variable temperature at bottom wall.

In numerous industrial and manufacturing process, liquids are used to control heat exchange. Several liquids (may be single or two phase) such as water, engine oil, kerosene oil, ethylene glycol, water–glycol and propylene glycol are used as a heat transfer agent in the industry (in the polymer extraction, paper production, power generation, glass fibers, etc), automobile, electronics and different engineering processes. Poor thermal conductivity may affect the heat transfer capability in a various industrial and cooling systems. The addition of ultrafine solid particles (nanometer sized) to conventional heat transfer liquids is quite useful in order to trigger thermal conductivity and heat transfer efficiency. It was found that the thermal properties of these fluids are remarkably enhanced. The nanoparticles mixed with base fluids may be metals (Ag, Cu, Al, etc) metal oxides (CuO, Al_2O_3, TiO_2, etc), nanotubes like carbon nanotubes (single and multi-wall) and carbides (SiC, TiC, etc). Maxwell [4] proposed a model for the enhancement of thermal conductivity by adding small particles. Masuda et al. [5] also presented experimental results that thermal conductivity can be improved by dispersing ultrafine particles in base fluids. Later on, it was Choi [6] who coined the name nanofluid and reported

experimentally that nanofluids have higher thermal conductivity and heat transfer capacity. Nanofluids have considerably revolutionized the modern technological world and are found to be the best coolant in the various engineering applications, such as in cooling of nuclear reactors [7], automotive [8, 9], electronic cooling [10–12], refrigerators [13–15], solar collectors [16, 17] and various heat exchangers [18, 19]. Since, nanofluid with astonishing heat transit characteristics is the most discoursed topic of the time, and as a result, has been receiving considerable attention, researchers and scientist are encouraged to explore emerging applications of nanofluids in different aspects. Sheikholeslami et al. [20] presented the convection phenomena in a porous medium enclosure containing nanofluid which is influenced by magnetic force. Saleem et al. [21] analyzed the important flow and thermal features of ferro-nanofluid in a porous medium cavity to involving radiation and electric force. Subhani and Nadeem [22] treated numerically micropolar hybrid nanofluid past an exponentially stretching surface, flow and thermal characteristics of this new class nanofluid are analyzed in the porous medium. Moreover, the addition of microorganism can improve the stability of nanofluid; in view of this, Lu et al. [23] searched out the flow and thermal behavior of nanofluid with gyrotactic microorganisms considering chemical reaction effect, influence by thermal radiation and boundary slip condition. Some recent investigations regarding applications of nanofluids in various aspects may be found [24–45].

Over the last few decades, the flow and heat transfer of nanofluids inside different cavities under various conditions have been investigated by many researchers. Some recent explorations include the review of rotating flow and variable thermal properties of hybrid nanoparticles with two different types of base fluids (water and ethylene glycol) presented by Usman et al. [46]. Chamkha and Selimefendigil [47] studied the entropy generation in the natural convective flow of nanofluid in a porous medium cavity; they concluded that heat transfer and entropy generation are enhanced because of increase in Darcy number and solid fraction of nanoparticles. Haq and Aman [48] studied flow and thermal behavior of nanofluid inside a trapezoidal cavity with heated object and found that nanoparticle volume fraction has a key role in thermal conductivity enhancement. Rahman et al. [49] scrutinized numerically the convective flow of nanofluid in closed geometry with porous medium subject to magnetic field and Arrhenius chemical reaction. Yanni and Xiaoming [50] inspected the nanofluid surface driven convection in a rectangular cavity and found that nanoparticles fraction greatly influenced the surface tension driven convection and intensity of heat transfer characteristics. In another study, Wang et al. [51] considered the impact of temperature-dependent flow and heat transfer properties on the power

law fluid in a rectangular cavity. The thermal properties of nanofluid under the impact of radiation heat source inside a wavy shape cavity are scrutinized by Alkanhal et al. [52]. Their obtained results point out that the Nusselt number enhances due to radiative heat exchange. The free convection of nanofluid in a cavity with porous medium is considered by Ahmed and Rashed [35]. The Buongiorno's model is proposed for nanofluid to investigate the flow field. The flow behavior and thermal distribution are subject to wavy boundary and magnetic field. Pal et al. [53] discussed the non-homogenous model for Cu–water nanofluid inside in a cavity with wavy-type wall. Haq et al. [54] described the thermal and flow properties in rhombus cavity filled with CuO–water nanofluid. The cavity contains square heated obstacle which controls the heat transfer characteristics in the cavity.

The present exploration focuses on the thermal and flow properties of CuO–water nanofluid inside a partially heated rectangular cavity. In the cavity, the flow field is subject to two heated wavy rods. Thus, our intention here is to examine the thermal and flow characteristics of nanofluid inside the rectangular cavity. In addition incorporating the flow under the influence of corrugated heated rods. The finite element method is applied to simulate the effect of various parameters on the governing problem. The article is put together as, in Sect. 2 details of the mathematical formulation have been discussed. Section 3 presents the proposed solution methodologies for the solution of governing partial differential equations. The numerical results and discussion are reported in Sect. 4. Finally, in Sect. 5, the paper is concluded with a discussion on the results.

Mathematical formulation

Consider the steady two-dimensional flow of Cu−water nanofluid in a partially heated rectangular cavity. The enclosure contains two heated corrugated rods with constant temperature T_h. The vertical walls of cavity are kept cold at constant temperature T_C. The outer heated boundaries of the cavity have a constant temperature T_h, while the remaining portions of the upper and lower wall are adiabatic. Figure 1 illustrates the

geometry of the problem. The mesh generation for the numerical procedure is given in Fig. 2. Triangular mesh is considered in the domain, and for better results and accuracy, we have generated maximum mesh at the inner heated rods. The flow field is controlled by external pressure gradient and buoyancy force. Also considering the natural convection here and applying the Oberbeck–Boussinesq approximation the buoyancy term. Under these assumptions, the governing problem obeys law of conservation of mass, momentum and energy as follows

$$\frac{\partial \overline{u}}{\partial \overline{x}} + \frac{\partial \overline{v}}{\partial \overline{y}} = 0, \tag{1}$$

$$\overline{u}\frac{\partial \overline{u}}{\partial \overline{x}} + \overline{v}\frac{\partial \overline{u}}{\partial \overline{y}} = -\frac{1}{\rho_{nf}}\frac{\partial \overline{p}}{\partial \overline{x}} + \nu_{nf}\left(\frac{\partial^2 \overline{u}}{\partial \overline{x}^2} + \frac{\partial^2 \overline{u}}{\partial \overline{y}^2}\right), \tag{2}$$

$$\begin{aligned}\overline{u}\frac{\partial \overline{v}}{\partial \overline{x}} + \overline{v}\frac{\partial \overline{v}}{\partial \overline{y}} &= -\frac{1}{\rho_{nf}}\frac{\partial \overline{p}}{\partial \overline{y}} + \nu_{nf}\left(\frac{\partial^2 \overline{v}}{\partial \overline{x}^2} + \frac{\partial^2 \overline{v}}{\partial \overline{y}^2}\right) \\ &+ \frac{(\rho\beta)_{nf}}{\rho_{nf}}g(\overline{T} - T_C),\end{aligned} \tag{3}$$

$$\overline{u}\frac{\partial \overline{T}}{\partial \overline{x}} + \overline{v}\frac{\partial \overline{T}}{\partial \overline{y}} = \frac{k_{nf}}{(\rho C_p)_{nf}}\left(\frac{\partial^2 \overline{T}}{\partial \overline{x}^2} + \frac{\partial^2 \overline{T}}{\partial \overline{y}^2}\right). \tag{4}$$

With the associated boundary conditions for rectangular cavity are stated as,

Temperature at lower and upper walls

$$\begin{cases} \overline{T} = T_h, & \text{at} \quad 0.0 \leq \overline{x} \leq \frac{7l}{10}, \overline{y} = 0.0. \\ \overline{T} = T_h, & \text{at} \quad \frac{13l}{10} \leq \overline{x} \leq \frac{20l}{10}, \overline{y} = l. \end{cases} \tag{5}$$

$$\begin{cases} \frac{\partial \overline{T}}{\partial n} = 0, & \text{at} \quad \frac{7l}{10} \leq \overline{x} \leq \frac{20l}{10}, \overline{y} = 0.0. \\ \frac{\partial \overline{T}}{\partial n} = 0, & \text{at} \quad 0.0 \leq \overline{x} \leq \frac{13l}{10}, \overline{y} = l. \end{cases} \tag{6}$$

Temperature at left and right walls

$$\overline{T} = T_C. \tag{7}$$

Temperature at the inner rods
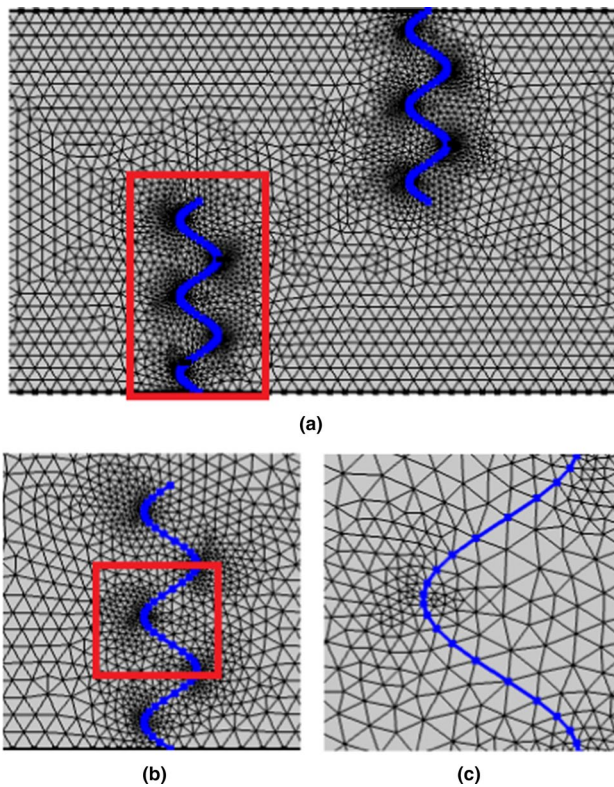
Fig. 1 Geometry of the physical problem

CuO−Water nanofluid

Heated wall $\overline{T} = \overline{T}_h$

Cold wall $\overline{T} = \overline{T}_c$

Adiabatic wall $\frac{\partial \overline{T}}{\partial n} = 0$
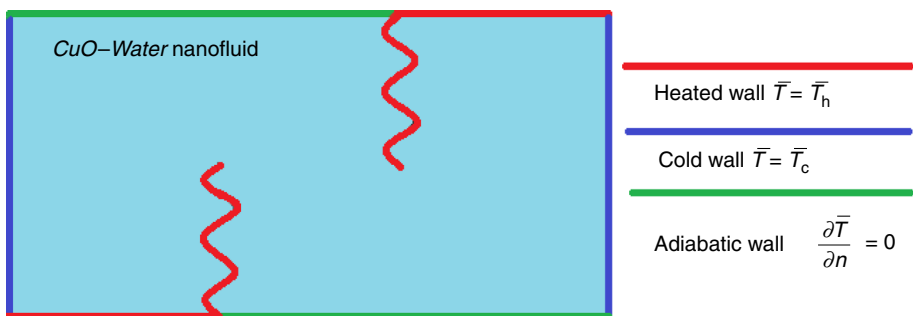
Fig. 2 Mesh generation at different portions in physical domain

$$\begin{cases} \overline{T} = T_{\text{h}}, & \text{at} \quad \overline{x} = \frac{7l}{10} + \lambda\sin\left(\frac{\omega\pi\overline{y}}{l}\right), 0.0 \leq \overline{y} \leq \frac{5l}{10}. \\ \overline{T} = T_{\text{h}}, & \text{at} \quad \overline{x} = \frac{13l}{10} + \lambda\sin\left(\frac{\omega\pi\overline{y}}{l}\right), \frac{5l}{10} \leq \overline{y} \leq l. \end{cases}$$ (8)

Velocity at all boundaries

$$\overline{u} = \overline{v} = 0.$$ (9)

Here, $(\overline{u}, \overline{v})$ are x and y components of velocity of the fluid and $\overline{T}$ denotes the temperature. ρ_{nf} is the effective density of nanofluid. ν_{nf} is the kinematic viscosities of nanofluid. $\left((\rho\beta)_{\text{nf}}, (\rho C_{\text{p}})_{\text{nf}}\right)$ represent thermal expansion coefficient and heat capacitance of nanofluid, whereas the thermal conductivity of nanofluid is given by k_{nf}, while T_{h} and T_{C} stand for temperature at heated and cold boundaries. λ and ω denote the amplitude and wavelength of the inner wavy heated rods. According to Koo–Kleinstreuer–Li, the thermal conductivity and dynamic viscosity are given as [4, 56, 57].

$$k_{\text{nf}} = k_{\text{static}} + k_{\text{Brownian}},$$

k_{static} is defined by Maxwell as

$$k_{\text{static}} = k_{\text{f}}\left(1 + \frac{3\left(\frac{k_{\text{s}}}{k_{\text{f}}} - 1\right)\phi}{\left(\frac{k_{\text{s}}}{k_{\text{f}}} + 2\right) - \left(\frac{k_{\text{s}}}{k_{\text{f}}} - 1\right)\phi}\right)$$

where the dynamic part is given by

$$k_{\text{Brownian}} = 5 \times 10^4 \phi(\rho C_{\text{p}})_{\text{f}}\sqrt{\frac{K_{\text{b}}T_0}{\rho_{\text{s}}D_{\text{s}}}}f(T_0, \phi)$$

Here, $K_{\text{b}}(= 1.38 \times 10^{-23}), T_0\left(= \frac{1}{2}(T_{\text{h}} - T_{\text{C}})\right), D_{\text{s}}$ symbolize Boltzmann constant, the average temperature and diameter of nanoparticles, here $f(T_0, \phi)$ is defined as

$$\begin{aligned} f(T_0, \phi) = 0.011(100\phi)^{-0.7272}\{(-6.04\phi + 0.4705)T_0 \\ + (1722.3\phi - 134.63)\}. \end{aligned}$$ (10)

Similarly, the viscosity due to Brownian motion is defined as

$$\mu_{\text{nf}} = \mu_{\text{static}} + \mu_{\text{Brownian}} = \frac{\mu_{\text{f}}}{(1 - \phi)^{2.5}} + \frac{k_{\text{Brownian}}}{k_{\text{f}}}\frac{\mu_{\text{f}}}{\text{Pr}},$$

The other thermodynamic properties are given by [58]

$$\begin{aligned} \rho_{\text{nf}} &= (1 - \phi)\rho_{\text{f}} + \phi\rho_{\text{s}}, \\ (\rho C_{\text{p}})_{\text{nf}} &= (1 - \phi)(\rho C_{\text{p}})_{\text{f}} + \phi(\rho C_{\text{p}})_{\text{s}}, \\ (\rho\beta)_{\text{nf}} &= (1 - \phi)(\rho\beta)_{\text{f}} + \phi(\rho\beta)_{\text{s}}. \end{aligned}$$ (11)

in which μ_{f} (= viscosity), ρ_{f} (= density) are the viscosity, of water, is given by β_{f} (= thermal expansion coefficient), and k_{f} (= thermal conductivity) of base fluid , whereas ϕ (= volume fraction), β_{s} (= thermal expansion coefficient), ρ_{s} (= density) , and k_{s} (= thermal conductivity) of nanoparticles.

Introducing the following dimensional variables [59, 60],

$$\begin{aligned} X &= \frac{\overline{x}}{l}, \quad Y = \frac{\overline{y}}{l}, \quad U = \frac{\overline{u}l}{\alpha_{\text{f}}} \quad V = \frac{\overline{v}l}{\alpha_{\text{f}}} \quad T = \frac{\overline{T} - T_{\text{c}}}{T_{\text{h}} - T_{\text{C}}} \\ P &= \frac{\overline{P}l^2}{\rho_{\text{f}}\alpha_{\text{f}}^2}, \quad \text{Pr} = \frac{\nu_{\text{f}}}{\alpha_{\text{f}}}, \quad \text{Ra} = \frac{\beta_{\text{f}}(T_{\text{h}} - T_{\text{C}})l^3}{\nu_{\text{f}}\alpha_{\text{f}}}. \end{aligned}$$ (12)

Here, Pr and Ra define the Prandtl and Rayleigh number. Implementing these variables, the governing Eqs. (2)–(4) and the boundary conditions (5) to (9) reduce to the following dimensionless equations

$$U\frac{\partial U}{\partial X} + V\frac{\partial U}{\partial Y} = -A\frac{\partial P}{\partial X} + B\text{Pr}\left(\frac{\partial^2 U}{\partial X^2} + \frac{\partial^2 U}{\partial Y^2}\right),$$ (13)

$$\begin{aligned} U\frac{\partial V}{\partial X} + V\frac{\partial V}{\partial Y} &= -A\frac{\partial P}{\partial Y} + B\text{Pr}\left(\frac{\partial^2 V}{\partial X^2} + \frac{\partial^2 V}{\partial Y^2}\right) \\ &+ C\text{Ra}\,\text{Pr}\,T, \end{aligned}$$ (14)

$$U\frac{\partial T}{\partial X} + V\frac{\partial T}{\partial Y} = D\left(\frac{\partial^2 T}{\partial X} + \frac{\partial^2 T}{\partial Y^2}\right). \tag{15}$$

The boundary conditions take the form

$$\left.\begin{array}{ll} 0.0 \le X \le 0.7, & Y = 0.0 \\ 1.3 \le X \le 2.0, & Y = 1.0 \end{array}\right\} T = 1 \tag{16}$$

$$\left.\begin{array}{ll} 0.7 \le X \le 2.0, & Y = 0.0 \\ 0.0 \le X \le 1.3, & Y = 1.0 \end{array}\right\} \frac{\partial T}{\partial n} = 0. \tag{17}$$

Temperature at left and right walls

$$\left.\begin{array}{ll} 0.0 \le Y \le 1.0, & X = 0.0 \\ 0.0 \le Y \le 1.0, & X = 2.0 \end{array}\right\} T = 0. \tag{18}$$

Temperature at the inner rods

$$\left.\begin{array}{ll} X = 0.7 + A_{\mathrm{m}}\sin(n_1 \pi Y), & 0.0 \le Y \le 0.5 \\ X = 1.3 + A_{\mathrm{m}}\sin(n_1 \pi Y), & 0.5 \le Y \le 1.0 \end{array}\right\} T = 1. \tag{19}$$

Velocity at all boundaries

$$U = V = 0. \tag{20}$$

In the above equation, the dimensionless physical parameters are defined as

$$A = \frac{\rho_{\mathrm{f}}}{\rho_{\mathrm{nf}}}, \quad B = \frac{A}{(1-\phi)^{2.5}} + \frac{A \times k_{\mathrm{Brownian}}}{\mathrm{Pr}\, k_{\mathrm{f}}} \tag{21}$$

$$D = \frac{(\rho C_{\mathrm{p}})_{\mathrm{f}}}{(\rho C_{\mathrm{p}})_{\mathrm{nf}}} + \frac{(\rho C_{\mathrm{p}})_{\mathrm{f}}}{(\rho C_{\mathrm{p}})_{\mathrm{nf}}}\left(\frac{k_{\mathrm{static}}}{k_{\mathrm{f}}} - 1\right) + \frac{(\rho C_{\mathrm{p}})_{\mathrm{f}}}{(\rho C_{\mathrm{p}})_{\mathrm{nf}}}\frac{k_{\mathrm{Brownian}}}{k_{\mathrm{f}}} \tag{22}$$

$$C = A\left(1 - \phi + \phi\frac{(\rho\beta)_{\mathrm{s}}}{(\rho\beta)_{\mathrm{f}}}\right), \quad A_{\mathrm{m}} = \frac{\lambda}{l}, \tag{23}$$

in which A, B, C and D are dimensionless thermophysical parameters where A_{m} and n_1 are the amplitude ratio and dimensionless wavelength number.

The quantity of physical interest, i.e., the heat transfer coefficient in terms of local and mean Nusselt number along the heated portions of the cavity is defined as

$$\mathrm{Nu} = -\frac{k_{\mathrm{nf}}}{k_{\mathrm{f}}}\frac{\partial T}{\partial n}\bigg|_{\mathrm{wall}} \quad \mathrm{Nu_m} = \int_s \mathrm{Nu}\, ds. \tag{24}$$

Here, n is the normal direction to the heated surface. s denotes the heated surface; for inner rods, s is length along the wavy rods.

Solution methodology

The system of partial differential equations (13)–(15) subject to the boundary conditions (16)–(20) is solved numerically incorporating finite element method (FEM) along with standard Galerkin technique. (see [61, 62]). We have two unknowns in the momentum equations (13) and (14), i.e., the velocity and pressure. Thus, to eliminate the pressure term, the standard penalty function formulation is added to the Galerkin mechanism, in which the pseudo-constitutive relation $P = -\gamma\left(\frac{\partial U}{\partial X} + \frac{\partial V}{\partial Y}\right)$ replaces the pressure term from (13), (14), where γ is penalty parameter ranges from $\left(10^6 - 10^8\right)$. The details of penalty function formulation may be found in [63] and [64]. Since γ is large number, the continuity equation (12) is satisfied, whereas the momentum equations in only unknown velocity components become

$$U\frac{\partial U}{\partial X} + V\frac{\partial U}{\partial Y} = A\gamma\frac{\partial}{\partial X}\left(\frac{\partial U}{\partial X} + \frac{\partial V}{\partial Y}\right) + B\mathrm{Pr}\left(\frac{\partial^2 U}{\partial X^2} + \frac{\partial^2 U}{\partial Y^2}\right), \tag{25}$$

$$U\frac{\partial V}{\partial X} + V\frac{\partial V}{\partial Y} = A\gamma\frac{\partial}{\partial Y}\left(\frac{\partial U}{\partial X} + \frac{\partial V}{\partial Y}\right) + B\mathrm{Pr}\left(\frac{\partial^2 V}{\partial X^2} + \frac{\partial^2 V}{\partial Y^2}\right) + C\mathrm{Ra}\,\mathrm{Pr}\,T, \tag{26}$$
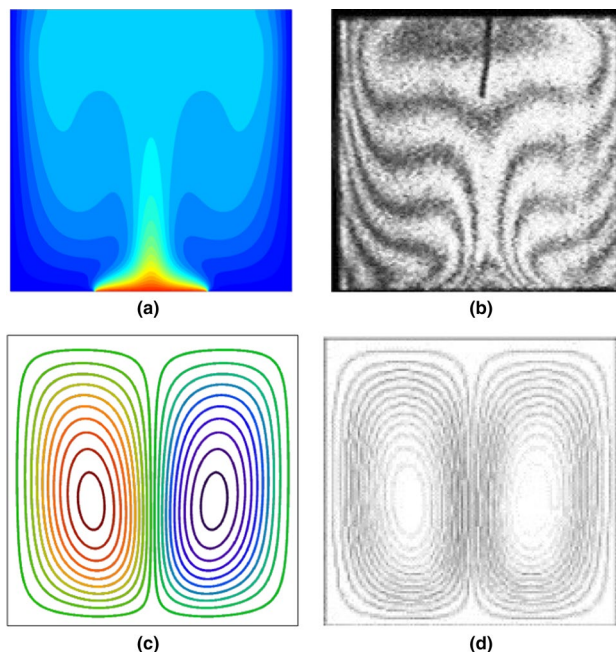

Fig. 3 Comparison of the present work **a** isotherms **c** streamlines with previous experimental (**b**) and numerical (**d**) results by Calcagni et al. [55] for Ra $= 1.86 \times 10^5$, $\phi = 0$
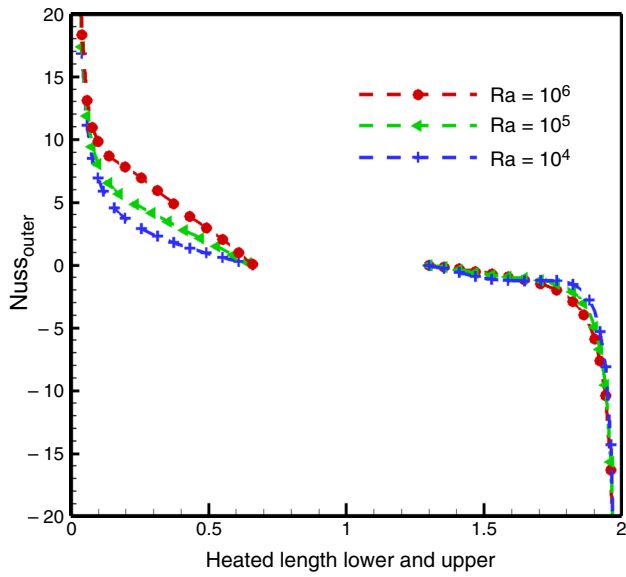
Fig. 4 Impact of Ra on Nusselt number along the outer heated length
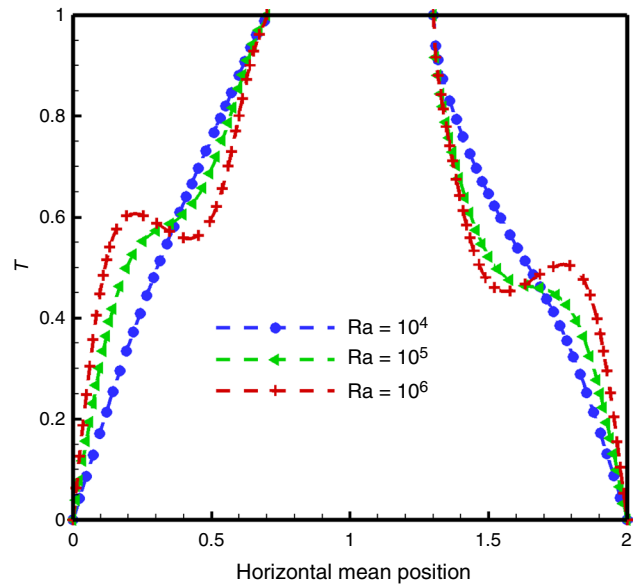

Fig. 6 Temperature profile for different Ra

The following basic steps are involved in the numerical method (FEM).

- The solution domain is divided into finite number of sub-domain; these finite elements formed finite element mesh. Here, we have discretized the domain into triangular element mesh as in Fig. 2.

- From the mesh element, equations are formed utilizing Galerkin approach, in which the approximate solution is assumed to each element in the domain.
- The global equation system for the whole domain is formed by combining all the local element equations.
- After assembling the element equations, the boundary conditions are imposed and the global equation system is then solved iteratively.
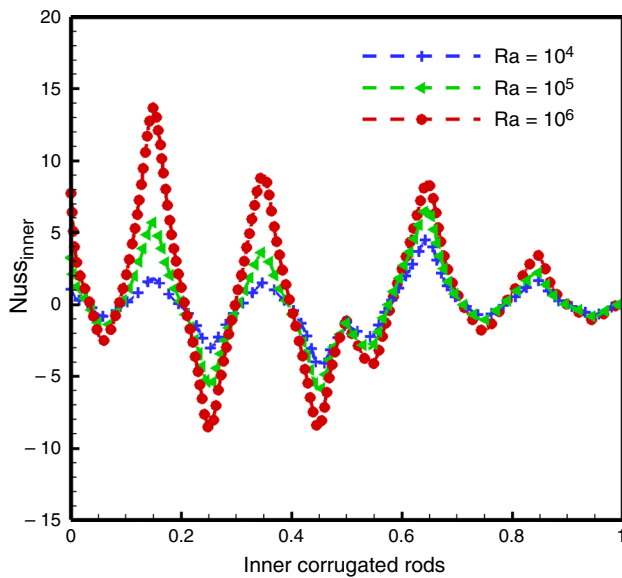
Fig. 5 Impact of Ra Nusselt number along the inner corrugated heated rods
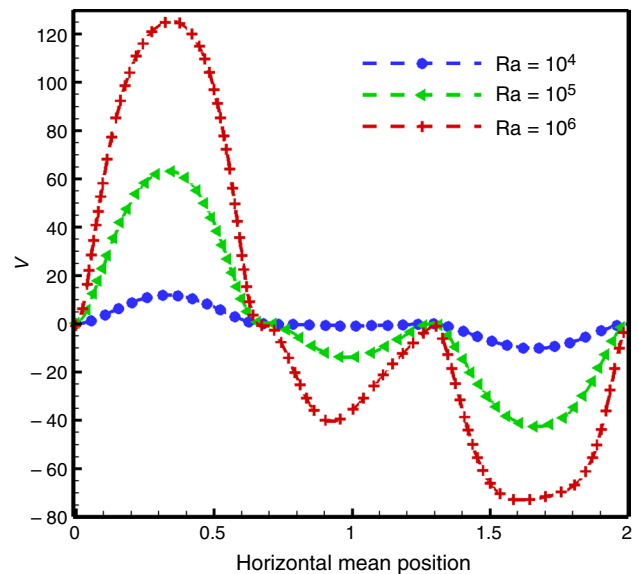
Fig. 7 Influence of Ra on velocity profile
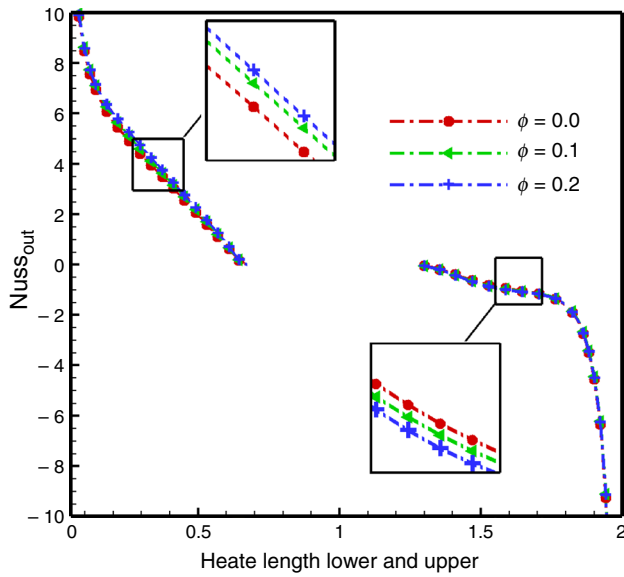
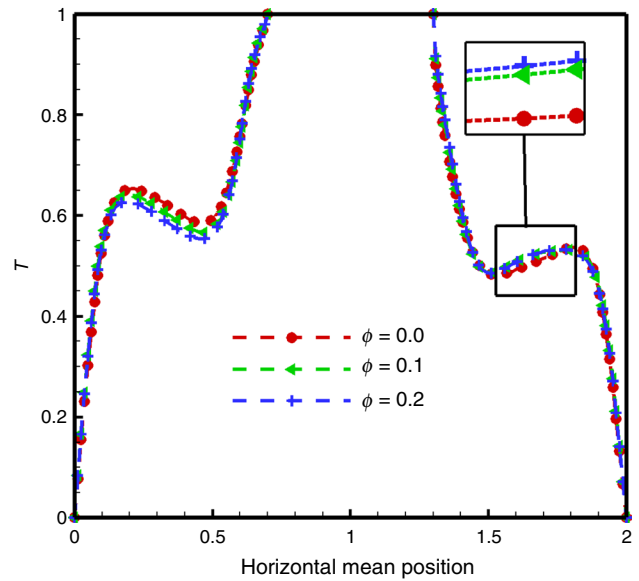**Fig. 8** Impact of ϕ on Nusselt number at outer heated cavity

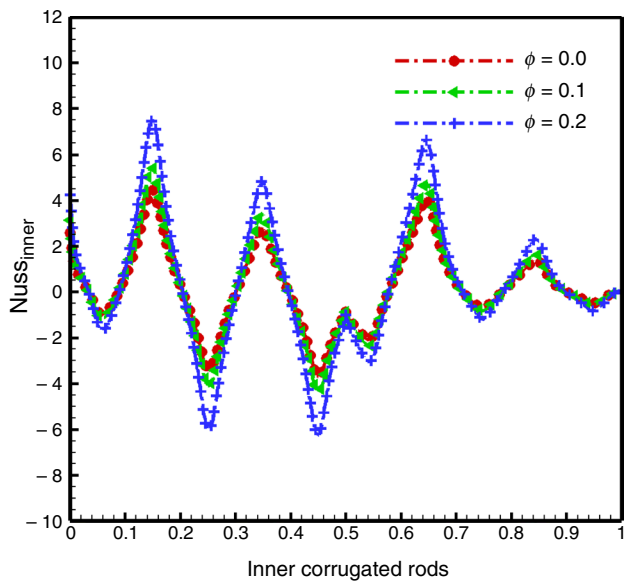**Fig. 10** Influence of ϕ on temperature profile

Fig. 9 Impact of ϕ on Nusselt number at inner heated rods
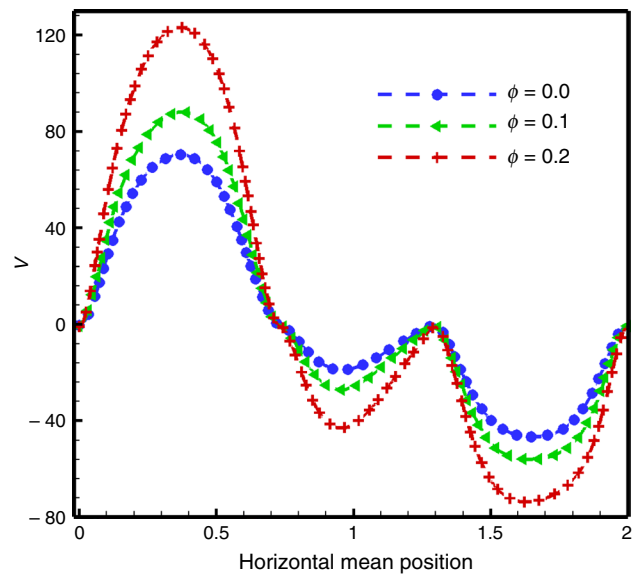

Fig. 11 Influence of ϕ on velocity distribution

Results and discussion

The natural convection heat transfer inside a rectangular cavity filled with CuO–water nanofluid is analyzed here. The cavity is partially heated at lower left (0.0–0.7) and upper right (1.3–2.0). The flow and heat transfer characteristics are affected by two wavy rods at position (0.7, 0.0) on the lower wall and at position (1.3, 1.0) on the upper wall. The finite element method is utilized to obtain the solution of the governing nonlinear partial differential equations. The

simulations are carried out for the influences of emerging physical parameters on the heat transfer rate, temperature and velocity distribution. Moreover, to validate our results, a comparison with previously publish experimental and numerical explorations by Calcagni et al. [55] is presented in Fig. 3. It can be seen from figure that our results shows strong resemblance with the experimental and numerical outcomes for isotherms and streamlines. The flow field
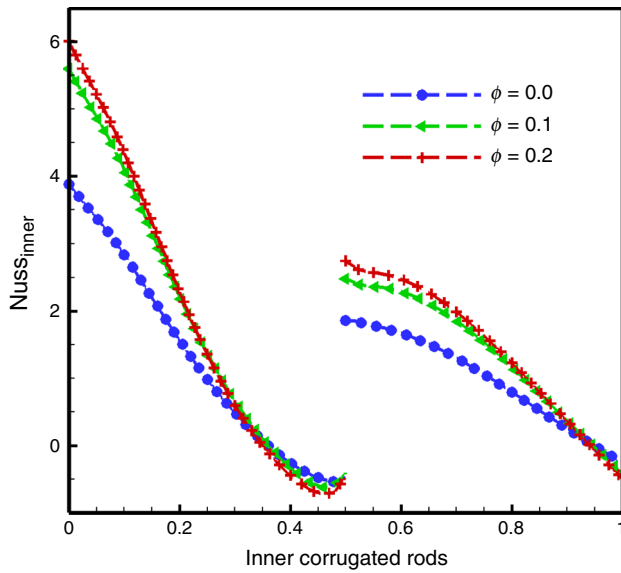
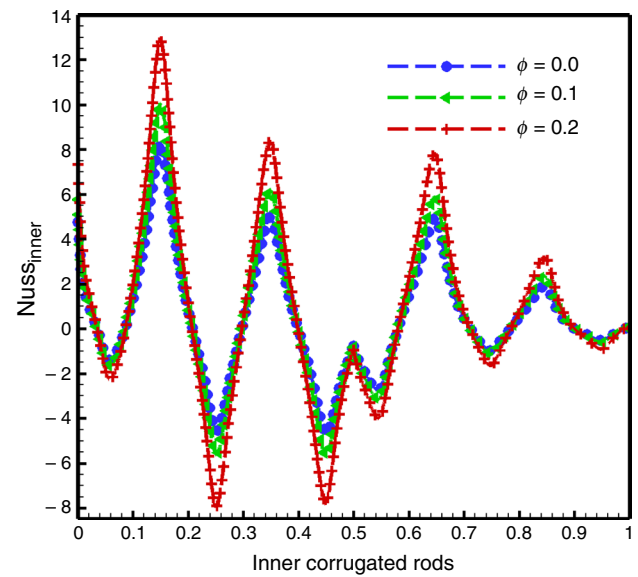**Fig. 12** Variations in Nusselt number for various ϕ and at $n_1 = 0$

Fig. 14 Variations in Nusselt number for various ϕ and at $n_1 = 20$
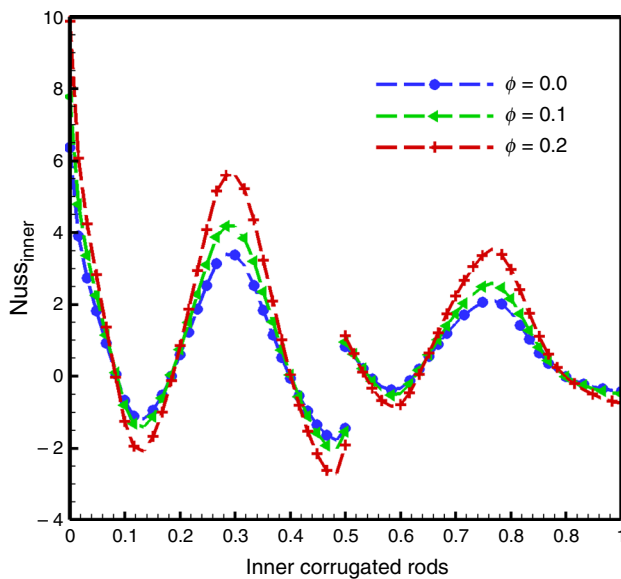

Fig. 13 Variations in Nusselt number for various ϕ and at $n_1 = 10$
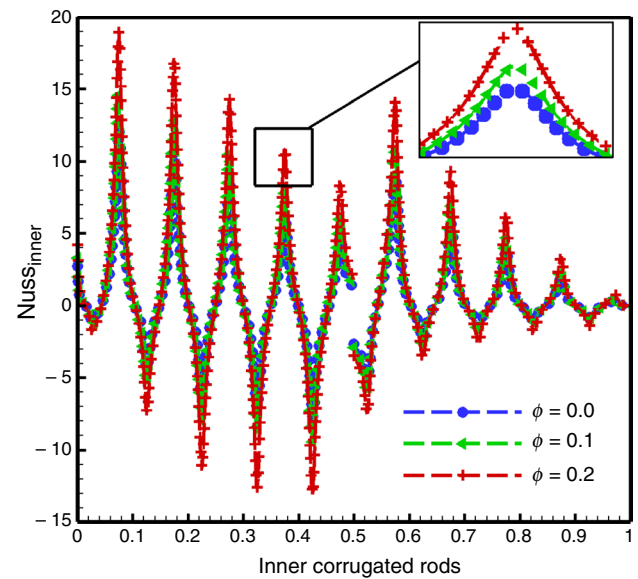

Fig. 15 Variations in Nusselt number for various ϕ and at $n_1 = 30$

results for different ranges [54] of Ra $(10^4–10^6)$, ϕ (0.0–0.2), A_m (0.05–0.2) and n (0–20) are disclosed in the following subsections.

Impact of Rayleigh number Ra

The influences of Rayleigh number on the flow field and heat transfer rate along the outer heated length and inner wavy rods are portrayed in Figs. 4–7. Figure 4 depicts the variations in heat transfer rate with respect to horizontal mean

position along the outer heated surface (upper and lower) of the cavity. It is noticed that local Nusselt number possesses maximum values for increasing Ra. Moreover, Fig. 4 illustrates that at lower heated length, the behavior of the heat transfer rate is increasing for Ra = 10^4 to 10^6 while, along the upper length it depicts lower values. The Nusselt number at the inner wavy heated rods for various Ra is presented in Fig. 5. A wavy behavior of the heat transfer rate can be observed from line graphs. Enhancement of heat transfer rate in a wavy pattern for higher Ra is evident from the figure. Since augmenting Rayleigh number, the buoyancy

Fig. 16 Isotherms for different Ra = 10^4 (left), Ra = 10^6 (right) and at various amplitudes $A_m = 0.05$ (**a**, **b**), $A_m = 0.1$ (**c**, **d**) and $A_m = 0.2$ (**e**, **f**)

(a)

(b)

(c)

(d)

(e)

(f)

Ra = 10^4

Ra = 10^6
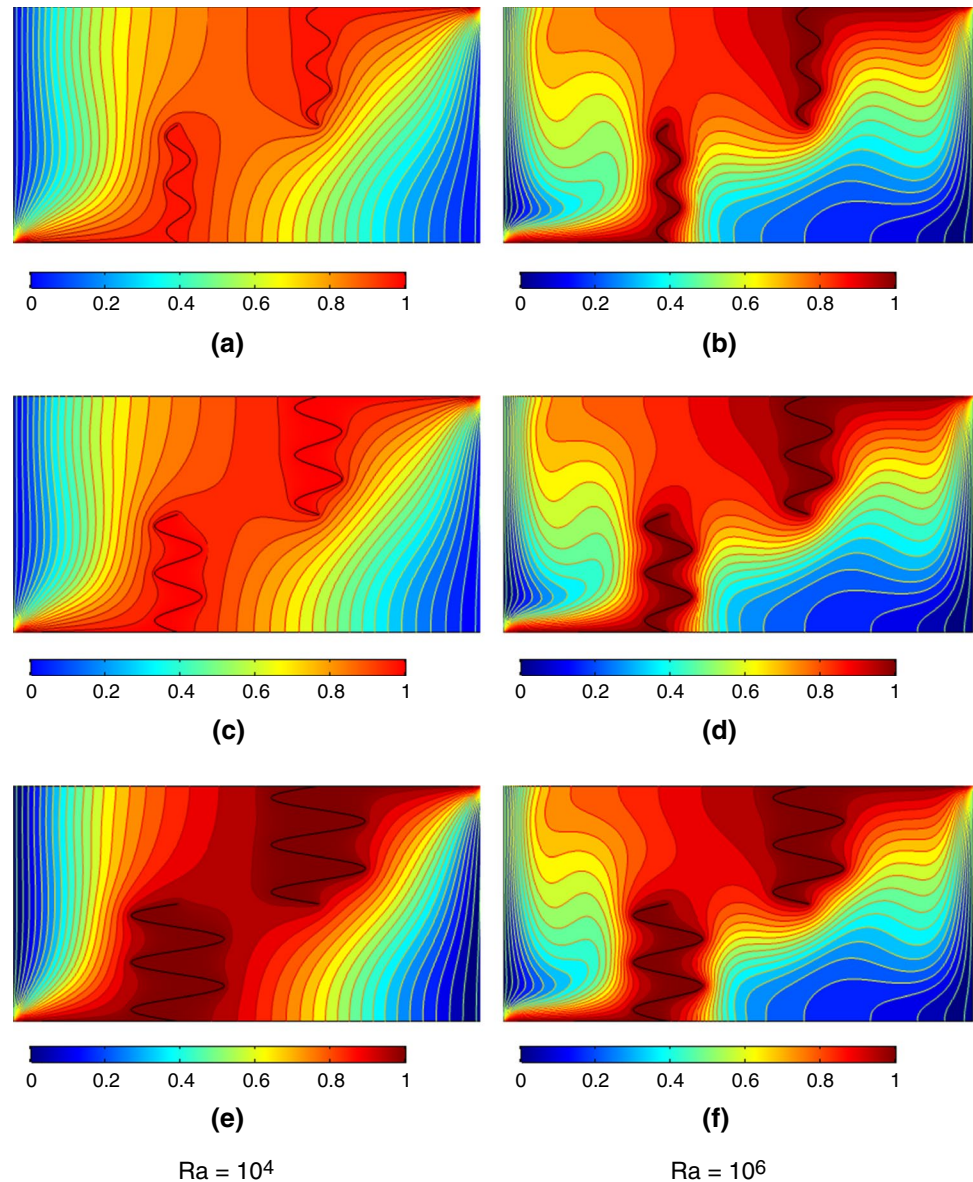
force becomes stronger and heat transfer takes place through convection. The alterations in temperature distribution along the horizontal mean position are presented in Fig. 6. This figure depicts that along the mean position from cold toward the lower heated rods the temperature has maximum values and start declines from the upper heated rod to the right cold surface. Further, from the figure, it can be noticed that the thermal boundary condition satisfies, i.e., the temperature is approaching 1. The vertical velocity along the horizontal mean position enhances from 0.0 to 0.7 and tends to decrease from 0.7 to 2.0 as evident from Fig. 7. Moreover, the figure clarifies that velocity converges to zero at all solid boundaries.

Impact of nanoparticles volume fraction ϕ

The variations in heat transfer rate, temperature and velocity profile at different nanoparticle volume fraction are presented in Figs. 8–11. The Nusselt number at outer heated length is exhibited in Fig. 8. It is observed heat transfer rate along the horizontal central line from (0.0–0.7) rises with respect to the addition of nanoparticles. On the other hand, from (1.3–2.0), Nusselt number gives minimum values as the volume fraction of nanoparticles augments. Figure 9 depicts the heat transfer rate at the inner wavy heated rods. Clearly, the figure illustrates that heat transfer propagates in a wavy pattern. Also, it can be noted that Nusselt number maximize by adding nanoparticles. Since the presence of nanoparticles provokes the effective viscosity and thermal conductivity of nanoparticles.

Fig. 17 Streamlines at various amplitudes $A_m = 0.05$ (**a**, **b**), $A_m = 0.1$ (**c**, **d**) and $A_m = 0.2$ (**e**, **f**) for different $Ra = 10^4$ (left), $Ra = 10^6$ (right)

(a)

(b)

(c)

(d)

(e)

(f)

$Ra = 10^4$

$Ra = 10^6$
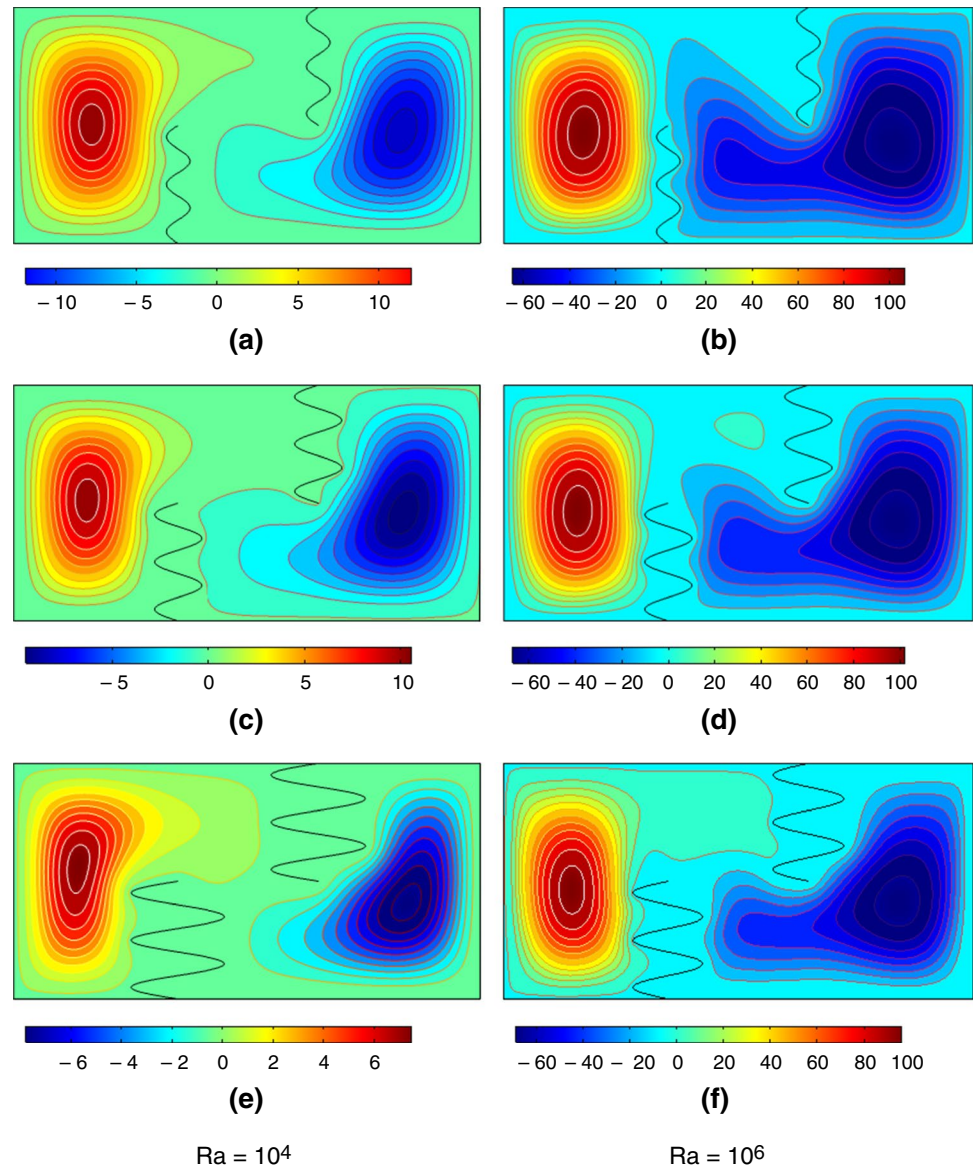
Higher thermal conductivity corresponds to the maximum heat transfer rate, while higher viscosity implies minimum heat transfer. Hence, we have from Figs. 8, 9 the effect of thermal conductivity is dominant over dynamic viscosity; thus, the net heat transfer rate escalates by the addition of nanoparticles. Figure 10 demonstrate the changes in temperature profile along the horizontal mean position. It is evident from the figure that between the mean position (0.0−0.7), temperature declines, while it rises between 1.3 and 2.0 as ϕ augments. The variations in velocity distribution with ϕ are presented in Fig. 11. The velocity field along the horizontal mean position gives maximum values from 0.0 to 0.7 and least values between 0.7 and 2.0.

Impact of wavelength number *n*

Figures 12–15 are considered for the combined effects of wavelength number *n* and nanoparticle volume fraction ϕ on heat transfer rate at inner heated rods. It is observed from Fig. 12 that for $n = 0$ (flat rods) the heat transfer rate enhances as the volume fraction of nanoparticle increases. The heat transfer rate along the heated rods at $n (= 5, 10, 20)$ is presented in Figs. 13–15, overall, at various corrugation, the Nusselt number escalates in a wavy manner for different ϕ. As the corrugation of the heated rods increases, the flow and thermal distribution adjacent to the rods varies. This gives rise in heat transfer rate through convection in the cavity. Thus, as the nanoparticle volume fraction increases, the effect of corrugation on heat transfer is more prominent.

Impact of amplitude A_m

The effects of varying amplitude A_m of the inner wavy rods on the flow and thermal fields at distinct Rayleigh number Ra are illustrated in Figs. 16 and 17. The isotherms are presented in Fig. 16a–f for $0.05 \leq A_m \leq 0.2$ at Ra = 10^4 and 10^6. Figure 16 reveals that as the amplitude of the inner wavy rods maximizes, the thermal contours intensify. This impact is more stronger for larger Rayleigh number Ra, i.e., at Ra = 10^6. Since, as A_m increases the space near the heated rods reduces for the circulations adjacent to the rods. Thus, the temperature contours are pushed toward the cold and adiabatic boundaries. This predicts that the temperature of the cavity overall rises, which is evident from Fig. 16a–f as the anticlockwise orientations getting stronger as both the amplitude and Rayleigh number vary. This confirms that heat transfer in the cavity is controlled by convection. On the other hand, the influences of different amplitude and Rayleigh number on streamlines pattern are depicted in Fig. 17a–f. The flow pattern in symmetric clockwise and anticlockwise can be observed. As the amplitude A_m increases the anticlockwise circulation getting stronger, while the clockwise orientations tend to decrease. Moreover, at smaller values of Ra, the streamline contours are weaker and its value is up to (-60). While at Ra = 10^6, the contours are stronger having values up to (100).

Conclusions

A numerical investigations of water-based CuO nanofluid in a rectangular cavity with heated wavy rods was studied in this article. The cavity is partially heat at lower left (at position $0.0-0.7$) and upper right (at position $1.3-2.0$) wall. The finite element method was employed to modeled physical problem in the form of governing partial differential equations. The simulations were executed for different Rayleigh number, nanoparticle volume fraction, wavelength number and at various amplitudes of inner wavy rods. The main findings of the present work are the maximum values of temperature, heat transfer rate both at outer heated length and inner corrugated rods is observed as Rayleigh number augments, higher Rayleigh number corresponds to convective heat transfer. Stronger Rayleigh number possesses maximum velocity distribution values (between 0.0 and 0.7) and lower values (between 1.3 and 2.0) along the central line of the cavity. The nanoparticle volume fraction also influences stronger behavior on heat transfer rate along the outer and inner heated rods, thermal and flow field. Along the horizontal mean position, the velocity exhibits maximum values between 0.0 and 0.7 and lesser values between 1.3 and 2.0. The impact of frequency number of the inner wavy

rods on flow and thermal field also found significant. The amount of heat transfer rate increases as the corrugation of the inner rods multiply. Thermal behavior corresponding to amplitude of inner rods gets maximized as the amplitude increases; thermal contour depicts that at higher amplitude and maximum Rayleigh number the heat transfer is fully controlled by convection as compared to lesser values of Rayleigh number. On the other hand, in the flow pattern, the clockwise orientation of the streamlines tends to reduce, while the clockwise circulation gets stronger at maximum values of both amplitude and Rayleigh number.

References

1. Sheikholeslami M, Gorji-Bandpy M, Pop I, Soleimani Soheil. Numerical study of natural convection between a circular enclosure and a sinusoidal cylinder using control volume based finite element method. Int J Therm Sci. 2013;72:147–58.
2. Wu F, Wang G. Numerical simulation of natural convection in an inclined porous cavity under time-periodic boundary conditions with a partially active thermal side wall. RSC Adv. 2017;7(28):17519–30.
3. Aparna K, Seetharamu KN. Investigations on the effect of non-uniform temperature on fluid flow and heat transfer in a trapezoidal cavity filled with porous media. Int J Heat Mass Transf. 2017;108:63–78.
4. Maxwell JC. A treatise on electricity and magnetism, vol. 1. Oxford: Clarendon Press; 1873.
5. Masuda H, Ebata A, Teramae K. Alteration of thermal conductivity and viscosity of liquid by dispersing ultra-fine particles (dispersion of γ-Al$_2$O$_3$, SiO$_2$ and TiO$_2$ ultra-fine particles). Netsu Bussei (Japan) 4227233; 1993.
6. Choi SUS. Enhancing conductivity of fluids with nanoparticles, ASME fluid eng. Division. 1995;231:99–105.
7. Barrett TR, Robinson S, Flinders K, Sergis A, Hardalupas Y. Investigating the use of nanofluids to improve high heat flux cooling systems. Fusion Eng Des. 2013;88(9–10):2594–7.
8. Leong KY, Saidur R, Kazi SN, Mamun AH. Performance investigation of an automotive car radiator operated with nanofluid-based coolants (nanofluid as a coolant in a radiator). Appl Therm Eng. 2010;30(17–18):2685–92.
9. Hussein AM, Bakar RA, Kadirgama K. Study of forced convection nanofluid heat transfer in the automotive cooling system. Case Stud Therm Eng. 2014;2:50–61.
10. Turgut A, Elbasan E. Nanofluids for electronics cooling. In: 2014 IEEE 20th international symposium for design and technology in electronic packaging (SIITME). IEEE; 2014. p. 35–37.
11. Hsieh SS, Leu HY, Liu HH. Spray cooling characteristics of nanofluids for electronic power devices. Nanoscale Res Lett. 2015;10(1):139.
12. Ijam A, Saidur R. Nanofluid as a coolant for electronic devices (cooling of electronic devices). Appl Therm Eng. 2012;32:76–82.
13. Bi S, Guo K, Liu Z, Wu J. Performance of a domestic refrigerator using TiO$_2$-R600a nano-refrigerant as working fluid. Energy Convers Manag. 2011;52(1):733–7.
14. Saidur R, Kazi SN, Hossain MS, Rahman MM, Mohammed HA. A review on the performance of nanoparticles suspended with refrigerants and lubricating oils in refrigeration systems. Renew Sustain Energy Rev. 2011;15(1):310–23.

15. Mahbubul IM, Saidur R, Amalina MA. Thermal conductivity, viscosity and density of R141b refrigerant based nanofluid. Proc Eng. 2013;56:310–5.

16. Saidur R, Meng TC, Said Z, Hasanuzzaman M, Kamyar A. Evaluation of the effect of nanofluid-based absorbers on direct solar collector. Int J Heat Mass Transf. 2012;55(21–22):5899–907.

17. Kasaeian A, Eshghi AT, Sameti M. A review on the applications of nanofluids in solar energy systems. Renew Sustain Energy Rev. 2015;43:584–98.

18. Kumar V, Tiwari A Kumar, Ghosh S K. Application of nanofluids in plate heat exchanger: a review. Energy Convers Manag. 2015;105:1017–36.

19. Said Z, Saidur R, Sabiha MA, Hepbasli A, Rahim NA. Energy and exergy efficiency of a flat plate solar collector using ph treated Al_2O_3 nanofluid. J of Clean Prod. 2016;112:3915–26.

20. Sheikholeslami M, Shehzad SA, Li Z, Shafee A. Numerical modeling for alumina nanofluid magnetohydrodynamic convective heat transfer in a permeable medium using Darcy law. Int J Heat Mass Transf. 2018;127:614–22.

21. Saleem S, Shafee A, Nawaz M, Dara RN, Tlili I, Bonyah E. Heat transfer in a permeable cavity filled with a ferrofluid under electric force and radiation effects. AIP Adv. 2019;9(9):095107.

22. Subhani M, Nadeem S. Numerical analysis of micropolar hybrid nanofluid. Appl Nanosci. 2019;9:447. https://doi.org/10.1007/s13204-018-0926-2.

23. Lu D, Ramzan M, Ullah N, Chung JD, Farooq U. A numerical treatment of radiative nanofluid 3D flow containing gyrotactic microorganism with anisotropic slip, binary chemical reaction and activation energy. Sci Rep. 2017;7(1):17008.

24. Hayat T, Nadeem S, Khan AU. Numerical analysis of Ag–Cuo/water rotating hybrid nanofluid with heat generation/absorption. Can J Phys. 2018;97:644–50.

25. Irshad N, Saleem A, Nadeem S, Shahzadi I. Endoscopic analysis of wave propagation with Ag-nanoparticles in curved tube having permeable walls. Curr Nanosci. 2018;14(5):384–402.

26. Nadeem S, Ahmed Z, Saleem S. Carbon nanotubes effects in magneto nanofluid flow over a curved stretching surface with variable viscosity. Microsyst Technol. 2019;25:2881. https://doi.org/10.1007/s00542-018-4232-4.

27. Ramzan M, Ullah N, Chung JD, Lu D, Farooq U. Buoyancy effects on the radiative magneto micropolar nanofluid flow with double stratification, activation energy and binary chemical reaction. Sci Rep. 2017;7(1):12901.

28. Mebarek-Oudina F. Convective heat transfer of Titania nanofluids of different base fluids in cylindrical annulus with discrete heat source. Heat Transf Asian Res. 2018;48:135–47.

29. Nayak MK, Bhatti M Mubashir, Makinde OD, Akbar NS. Transient magneto-squeezing flow of Nacl-CNP nanofluid over a sensor surface inspired by temperature dependent viscosity. In: Defect and diffusion forum, vol 387. Trans Tech Publications; 2018. p. 600–614.

30. Ellahi R, Zeeshan A, Hussain F, Abbas T. Study of shiny film coating on multi-fluid flows of a rotating disk suspended with nano-sized silver and gold particles: a comparative analysis. Coatings. 2018;8(12):422.

31. Javed MF, Khan NB, Khan MI, Muhammad R, Rehman MU, Khan SW, Khan TA, Hassan MT. Optimization of SWCNTs and MWCNTs (single and multi-wall carbon nanotubes) in peristaltic transport with thermal radiation in a non-uniform channel. J Mol Liq. 2019;273:383–91.

32. Nawaz M, Saleem S, Rana S. Computational study of chemical reactions during heat and mass transfer in magnetized partially ionized nanofluid. J Braz Soc Mech Sci Eng. 2019;41(8):326.

33. Sadiq MA, Khan AU, Saleem S, Nadeem S. Numerical simulation of oscillatory oblique stagnation point flow of a magneto micropolar nanofluid. RSC Adv. 2019;9(9):4751–64.

34. Saleem S, Nadeem S, Rashidi MM, Raju CSK. An optimal analysis of radiated nanomaterial flow with viscous dissipation and heat source. Microsyst Technol. 2019;25(2):683–9.

35. Ahmed SE, Rashed ZZ. MHD natural convection in a heat generating porous medium-filled wavy enclosures using Buongiorno's nanofluid model. Case Stud Therm Eng. 2019;14:100430.

36. Vo DD, Saleem S, Alderremy AA, Nguyen TK, Nadeem S, Li Z. Heat transfer enhancement and migration of ferrofluid due to electric force inside a porous media with complex geometry. Phys Scr. 2019;94:115218.

37. Saleem S, Rafiq H, Al-Qahtani A, El-Aziz MA, Malik MY, Animasaun IL. Magneto Jeffrey nanofluid bioconvection over a rotating vertical cone due to gyrotactic microorganism. Math Probl Eng. 2019;2019:3478037. https://doi.org/10.1155/2019/3478037

38. Ahmed Z, Al-Qahtani A, Nadeem S, Saleem S. Computational study of MHD nanofluid flow possessing micro-rotational inertia over a curved surface with variable thermophysical properties. Processes. 2019;7(6):387.

39. Sheikholeslami M, Shamlooei M. Fe_3O_4–H_2O nanofluid natural convection in presence of thermal radiation. Int J Hydrog Energy. 2017;42(9):5708–18.

40. Sheikholeslami M, Vajravelu K. Nanofluid flow and heat transfer in a cavity with variable magnetic field. Appl Math Comput. 2017;298:272–82.

41. Sheikholeslami M, Zeeshan A. Analysis of flow and heat transfer in water based nanofluid due to magnetic field in a porous enclosure with constant heat flux using CVFEM. Comput Methods Appl Mech Eng. 2017;320:68–81.

42. Sheikholeslami M, Arabkoohsar A, Jafaryar M. Impact of a helical-twisting device on the thermal–hydraulic performance of a nanofluid flow through a tube. J Therm Anal Calorim. 2019. https://doi.org/10.1007/s10973-019-08683-x

43. Sheikholeslami M. Solidification of NEPCM under the effect of magnetic field in a porous thermal energy storage enclosure using CuO nanoparticles. J Mol Liq. 2018;263:303–15.

44. Sheikholeslami M. Magnetic field influence on CuO–H_2O nanofluid convective flow in a permeable cavity considering various shapes for nanoparticles. Int J Hydrog Energy. 2017;42(31):19611–21.

45. Sheikholeslami M, Jafaryar M, Ali JA, Hamad SM, Divsalar A, Shafee A, Nguyen-Thoi T, Li Z. Simulation of turbulent flow of nanofluid due to existence of new effective turbulator involving entropy generation. J Mol Liq. 2019;291:111283.

46. Usman M, Hamid M, Zubair T, Haq RU, Wang W. Cu–Al_2O_3/water hybrid nanofluid through a permeable surface in the presence of nonlinear radiation and variable thermal conductivity via LSM. Int J Heat Mass Transf. 2018;126:1347–56.

47. Chamkha AJ, Selimefendigil F. MHD free convection and entropy generation in a corrugated cavity filled with a porous medium saturated with nanofluids. Entropy. 2018;20(11):846.

48. Haq RU, Aman S. Water functionalized CuO nanoparticles filled in a partially heated trapezoidal cavity with inner heated obstacle: FEM approach. Int J Heat Mass Transf. 2019;128:401–17.

49. Rahman MM, Pop I, Saghir MZ. Steady free convection flow within a titled nanofluid saturated porous cavity in the presence of a sloping magnetic field energized by an exothermic chemical reaction administered by Arrhenius kinetics. Int J Heat Mass Transf. 2019;129:198–211.

50. Jiang Y, Zhou X. Analysis of flow and heat transfer characteristics of nanofluids surface tension driven convection in a rectangular cavity. Int J Mech Sci. 2019;153–154:154–63.

51. Wang L, Huang C, Yang X, Chai Z, Shi B. Effects of temperature-dependent properties on natural convection of power-law nanofluids in rectangular cavities with sinusoidal temperature distribution. Int J Heat Mass Transf. 2019;128:688–99.

52. Alkanhal TA, Sheikholeslami M, Usman Muhammad, Haq R U, Shafee A, Al-Ahmadi A S, Tlili I. Thermal management of MHD nanofluid within the porous medium enclosed in a wavy shaped cavity with square obstacle in the presence of radiation heat source. Int J Heat Mass Transf. 2019;139:87–94.

53. Pal SK, Bhattacharyya S, Pop I. A numerical study on non-homogeneous model for the conjugate-mixed convection of a Cu–water nanofluid in an enclosure with thick wavy wall. Appl Math Comput. 2019;356:219–34.

54. Haq RU, Soomro FA, Hammouch Z. Heat transfer analysis of CuO–water enclosed in a partially heated rhombus with heated square obstacle. Int J Heat Mass Transf. 2018;118:773–84.

55. Calcagni B, Marsili F, Paroncini M. Natural convective heat transfer in square enclosures heated from below. Appl Therm Eng. 2005;25(16):2522–31.

56. Koo J, Kleinstreuer C. A new thermal conductivity model for nanofluids. J Nanopart Res. 2004;6(6):577–88.

57. Li J. Computational analysis of nanofluid flow in microchannels with applications to micro-heat sinks and bio-MEMS. Raleigh: North Carolina State University; 2008. Ph.D. Thesis. http://www.lib.ncsu.edu/resolver/1840.16/4749

58. Ahmad S, Rohni AM, Pop I. Blasius and Sakiadis problems in nanofluids. Acta Mech. 2011;218(3–4):195–204.

59. Esfe MH, Arani AAA, Yan WM, Ehteram H, Aghaie A, Afrand M. Natural convection in a trapezoidal enclosure filled with carbon nanotube–EG–water nanofluid. Int J Heat Mass Transf. 2016;92:76–82.

60. Haq Rizwan Ul, Soomro Feroz Ahmed, F Öztop Hakan, Mekkaoui Toufik. Thermal management of water-based carbon nanotubes enclosed in a partially heated triangular cavity with heated cylindrical obstacle. Int J Heat Mass Transf. 2019;131:724–36.

61. Taylor C, Hood P. A numerical solution of the Navier–Stokes equations using the finite element technique. Comput Fluids. 1973;1:73–100.

62. Jiajan W. Solution to incompressible Navier Stokes equations by using finite element method 2010. Ph.D. Thesis.

63. Heinrich JC, Vionnet CA. The penalty method for the Navier–Stokes equations. Arch Comput Methods Eng. 1995;2(2):51–65.

64. Dyne BR, Heinrich JC. Physically correct penalt-like formulations for accurate pressure calculation in finite element algorithms of the Navier–Stokes equations. Int J Numer Methods Eng. 1993;36(22):3883–902.